Strain proportional damping in Bernoulli-Euler beam theory

Domenico Lisitano[a], Janko Slavič[b,*], Elvio Bonisoli[a], Miha Boltežar[b]

[a] *Politecnico di Torino, Department of Mechanical and Aerospace Engineering, Corso Duca degli Abruzzi 24, 10100 Torino, Italy*
[b] *University of Ljubljana, Faculty of Mechanical Engineering, Aškerčeva 6, 1000 Ljubljana, Slovenia*

Cite as:
Domenico Lisitano, Janko Slavič, Elvio Bonisoli, Miha Boltežar, Strain proportional damping in Bernoulli-Euler beam theory, Mechanical Systems and Signal Processing, Volume 145,2020,ISSN 0888-3270, https://doi.org/10.1016/j.ymssp.2020.106907

Abstract

In structural dynamics, different damping models are used; however, due to modal decomposition, those models typically result in the use of the damping ratio as the modal damping parameter. If proportional viscous damping is used, the damping ratio can be related to the mass and stiffness parameters of a particular dynamic system, i.e. the damping is structure-specific.

Lord Rayleigh introduced the idea of proportional damping based on the kinetic and potential energy of a dynamic system. If one imagines a particular deflection shape, then most of the kinetic energy is at the locations with high amplitudes of vibration and none at the nodes. As the potential energy is related to the strain, for a particular deflection shape, the displacement and strain deflection shapes do not correspond, and neither does the location of the kinetic and potential energy proportionality. The proportional damping is valid for the spatially-cumulative kinetic and potential energy, but questionable for a particular mode shape at a particular location.

Based on the Euler-Bernoulli beam theory, this research proposes an exten-

*Corresponding author
Email address: janko.slavic@fs.uni-lj.si (Janko Slavič)

sion to the proportional damping approach, which results in a material-specific damping parameter. It is shown that using this material damping parameter and the assumption of damping energy proportionality to the local modal strain energy, the modal damping ratio of each mode can be obtained theoretically. This finding was confirmed against several experimental test-cases.

The proposed material-specific damping parameter opens up the possibility to obtain the structure-specific damping parameters using the theoretical/numerical mode shapes.

Keywords: damping ratio, bending vibrations, material property, strain

1. Introduction

In vibrating systems, damping is the physical phenomenon responsible for the dissipation of energy. To obtain a system of uncoupled differential equations, the damping models typically used, do not correspond to physically observed phenomena [1, 2, 3, 4].

One of the first descriptions of damping was given by Lord Rayleigh [5], who discussed that due to internal damping, the mechanical energy *in vacuo* would finally be dissipated as heat. In the case of an open space, the interaction with the surrounding air would result in mathematical difficulties. Therefore, acceleration (mass) and velocity (stiffness) proportionality was introduced [5, 6]. It follows that the dissipated energy can be assumed to be proportional to the kinetic and the potential energy, making it possible to uncouple the equations of motion in the generalised coordinates, see, *e.g.*, Caughey *et al.* [7] or Adhikari [8]. Proportional viscous damping is usually described with α and β parameters, which are used with a particular natural frequency to define the damping ratio of a particular mode shape [9, 10]. The proportional viscous damping model is widely used and requires fitting the proportional viscous damping coefficients α and β to the experimental data of a particular structure. Such a description of damping is structure-specific and cannot be generalised to other structures [11, 12, 13]. When proportional viscous damping is applied to ho-

mogeneous structures, the mass proportional viscous damping coefficient α is usually neglected, see, *e.g.*, [11]. In fact, in most of the experimental campaigns, the damping ratios are linearly increasing with the frequency [14, 15, 16] and can be modelled using the stiffness viscous damping coefficient β, only.

Besides proportional viscous damping, hysteretic proportional damping was also researched [17, 18]. The strain-rate coefficient can be related to the complex Young's modulus using the loss factor [19]. The loss factor results, like the damping ratio, in a structure-specific damping estimation. A similar conclusion can be made for other methods based on the complex modulus model methods [20], *e.g.*, Golla-Hughes-McTavish [21], the elastic displacement fields [22], fractional derivatives [23], standard linear solid or Zener model [24].

If the above research was focused on relating damping to structural dynamics theory, then an equally important question is, what is the underlying physics of energy dissipation? Is it velocity, displacement, strain amplitude proportional? Maxwell, Boltzmann, Voigt and Kelvin researched in the nineteenth century the viscoelasticity and dissipative behaviour of solid metallic material. Bert [25] gave a comprehensive review of the material damping model for structural dynamics. Banks and Inman [26] compared the most used models for continuous beam systems, such as Kelvin-Voigt (or strain-rate) [27] and spatial hysteresis [28]; which are both frequency-dependent models. The energy dissipated by vibrating beams was related to the local rate of change of strains (Kelvin-Voigt) or beam-section rotations (spatial hysteresis), considered responsible for the internal friction in the material. The combination of the strain-rate damping model and fluid (commonly air) damping modifies the Rayleigh's damping ratio expression by introducing fluid-viscous-damping and strain-rate-damping proportionality. Kimball and Lovell [29] showed experimentally, in 1927, a correlation of the internal friction damping with the strain amplitude. In the 1950s, Lazan concluded that damping is proportional to the square of the strain amplitude [30].

Recently, Iglesias *et al.* [31] presented a method for the estimation of mass proportionality viscous damping coefficients from the free response of systems,

using a reduced-interface distribution analysis; Yılmaz *et al.* [32] predicted the viscous damping coefficients using a machine-learning-based method. Sarbinowski *et al.* [33] identified the Rayleigh viscous damping using a vision-based method. Hamdaoui *et al.* [34] identified the viscoelastic damping properties of a material using the adjoint method. Mei *et al.* [35] proposed a modified proportional viscous damping approach considering exponential damping, and Nghiem *et al.* [36] proposed a new 1-D damping model. Heitz *et al.* [37] proposed an equivalent evolving viscous damping ratio to model nonlinear damped structures. The damping properties of recent 3D printed material were investigated by Ficzere *et al.* [38].

It is commonly accepted that damping has to be derived from experimental data, fitting equivalent damping models, such as Rayleigh viscous damping or other physical damping models. However, material friction damping is related to the ability of the material to locally dissipate energy due to micro-slides during vibrations, *i.e.* to the local strain amplitude. The relation between the distribution of dissipation and strain field amplitude was theoretically and experimentally researched by Mihalec *et al.* [39], monitoring the surface temperature. Higher temperature increments correspond to higher strains; while energy is not locally dissipated at the node of the strain deformation. As Kranjc *et al.* [40] showed, the displacement mode shapes and the strain mode shapes do not correspond; due to this the location where the modal displacement/velocity is zero, does not correspond to the locations where the strain is zero. For an ideal system without damping the mechanical energy is conserved, but since the strain and displacement mode shapes do not correspond, this conservation is not valid at a particular location.

In this research, the dissipation property of the material is modelled with a time and spatially independent material property applied to the strain field of the system to obtain the modal damping ratio. The dissipation distribution is directly related to the strain field, and the energy dissipated from each mode is the integral contribution of the local dissipation. This research focuses on the Euler-Bernoulli beam theory, which enables a relatively clear analytical and ex-

perimental observation of the damping mechanism. The analytical background of the proposed approach is presented in Sec. 2. The concept of strain proportional damping is presented in Sec. 3 and developed for the beam case in Sec. 4. The experimental research and validation is then presented in Sec. 5. Finally, Sec. 6 drains the conclusion and future perspectives resulting from the considerations of this research.

2. Theoretical background

In a damping-free vibrating structure the mechanical energy is conserved and alternates between the maximum kinetic and the maximum potential energy, which are respectively defined as [41]:

$$E_k(t) = \frac{1}{2}\int_V \rho\, \dot{\boldsymbol{u}}(t)^T\, \dot{\boldsymbol{u}}(t)\, \mathrm{d}V, \qquad E_p(t) = \int_V \boldsymbol{\sigma}(t)^T\, \boldsymbol{\varepsilon}(t)\, \mathrm{d}V. \tag{1}$$

where ρ is the material density, $\dot{\boldsymbol{u}}$ is the local velocity vector, $\boldsymbol{\sigma}$ and $\boldsymbol{\varepsilon}$ are the local stress and strain vectors, respectively.

The potential $E_p(t)$ can be written as the sum of the potential energy related to each of the r^{th} mode shapes, using modal expansion or modal decomposition theorems [42, 43] :

$$E_p(t) = \sum_{r=1}^{\inf} E_p^r(t)\,. \tag{2}$$

Since the modal participation factors of high-frequency modes are usually negligible [44], only a limited number of modes is usually sufficient to represent almost the entire potential energy of the system. A similar conclusion could be made for the kinetic energy.

The dissipation properties of the system are usually introduced in the modal model to include dissipation effects, such as the damping ratio ζ_r or the loss factor η_r. One way of defining the damping ratio/loss factor in relation to the energy dissipated in a steady-state oscillating cycle with respect to the total energy or to the maximum of the potential energy $\hat{E}_p^r$ of the r^{th} mode shape: [45].

$$\zeta_r = \frac{\eta_r}{2} = \frac{W_d^r}{2\pi \hat{E}_p^r} \tag{3}$$

where W_d^r is the energy lost by the r^{th} mode shape in an oscillation cycle.

The other way (for proportional viscous damping) is to define the modal damping ratio ζ_r as [8]:

$$\zeta_r = \frac{\eta_r}{2} = \frac{1}{2}\left(\frac{\alpha}{\omega_r} + \beta\,\omega_r\right) \tag{4}$$

where α and β are, for a particular mechanical system, identified from an experiment.

A similar consideration could be given for other damping models.

3. Strain proportional damping

Eqs. (3) and (4) show that the damping ratio can be defined very differently and still be successfully used in numerical models as long as it is experimentally identified for a particular structure.

However, it is reasonable to expect that the internal material friction should be related to the microstructural properties of the material and the strain-stress field induced by the vibrating structure. This research introduces a new material property, denoted μ, which will be used to quantify the strain proportional damping. The mass matrix $\mathbf{M}$ is defined by the geometry and the material density ρ; the stiffness matrix $\mathbf{K}$ is defined by the geometry and modulus of elasticity E. Similarly, the description of damping should be defined with the geometry and the strain proportional damping parameter μ.

Dissipation is related to the micro-movements of the material under the strain field, and therefore to the strain energy. For a damping-free continuous system, the potential energy coincides with the strain energy of the system, *i.e.*, the energy stored in the system due to deformations (3). Strain energy is, therefore, a good indicator to quantify and localise the dissipation of energy.

For a linear, time-invariant system, the excitation at the r-th natural frequency $\omega_{n,r}$ results in the deflection with the r-th mode shape ϕ_r. This implies that the energy is lost only where the strain is not zero, as experimentally proved in [39].

In this research it is assumed that the dissipation of the internal energy (*i.e.*, the damping energy) is proportional to the strain energy; based on the above discussion the following assumption about the damping ratio is made:

$$\zeta_r = \mu \sqrt{\int_V \varepsilon^2 \, \mathrm{d}V} \tag{5}$$

where μ is the newly introduced, strain proportional material damping parameter. It is reasonable to expect that the proposed parameter μ can be assumed to be frequency independent [29, 46]. In Eq. (5) the square ε^2 is introduced in the analogy with the strain energy (which also accounts for the positive and negative strain ε). Due to the square root in Eq. (5) the damping ratio becomes strain-amplitude proportional.

4. Strain proportional damping in Euler-Bernoulli beam theory

The definition of the strain proportional damping ratio (5) is here applied to the free-free beam theory and the modal strain shapes of such a beam.

According to Euler-Bernoulli theory, the bending behaviour of a beam generates a strain field $\varepsilon_{xx}(x, z)$ [41]:

$$\varepsilon = \varepsilon_{xx}(x, z) = -\frac{\partial^2 w(x)}{\partial x^2} z \tag{6}$$

where $w(x)$ is the displacement of the beam due to the bending force and z is the distance from the middle plane, see Fig. 1.

Since interest is focused on the modal damping ratio ζ_r, the resonance conditions are studied. For bending around the y direction, the displacement of the r-th natural frequency is described using the r-th mass-normalised mode shape ϕ_r scaled with the constant scaling factor g_{yy} required to get the physical beam displacement in the z direction:

$$w_r(x) = g_{yy} \, \phi_r(x). \tag{7}$$

Inserting (7) into (6):

$$\varepsilon_{xx}(x, z) = -\frac{\partial^2 (g_{yy} \, \phi_r(x))}{\partial x^2} \, z \tag{8}$$

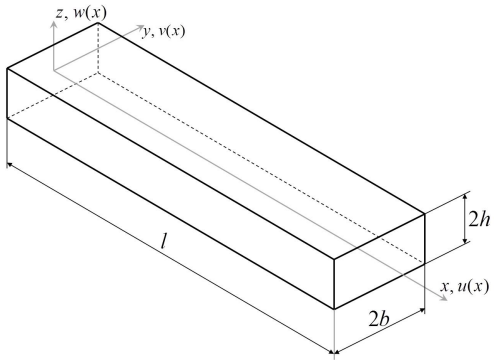

Figure 1: Beam schematic

where $\partial^2\phi_r/\partial x^2$ represents the r-th curvature mode shape [47].

Inserting Eq. (8) into Eq. (5) the rth damping ratio $\zeta_{r,y}$ for the bending vibrations around the y axis is:

$$\zeta_{r,y} = \mu \sqrt{\int_V g_{yy}^2 \left(\frac{\partial^2 \phi_r(x)}{\partial x^2}\, z \right)^2 \mathrm{d}V} \tag{9}$$

The curvature mode shape depends on the x coordinate only, and therefore the volume integral in Eq. (9) is simplified to a line integral along x:

$$\zeta_{r,y} = \mu \sqrt{I_{yy}\, g_{yy}^2 \int_0^l \left(\frac{\partial^2 \phi_r(x)}{\partial x^2} \right)^2 \mathrm{d}x} \tag{10}$$

where I_{yy} is the second moment of area A:

$$I_{yy} = \int_A z^2 \,\mathrm{d}A \tag{11}$$

and l is the beam length.

Eq. (10) can be related to the r-th modal strain energy (MSE) $\pi_{r,y}$ [41]:

$$\pi_{r,y} = \frac{1}{2}\, E\, I_{yy} \int_0^l \left(\frac{\partial^2 \phi_r(x)}{\partial x^2} \right)^2 \mathrm{d}x \tag{12}$$

With Eq. (10) the damping ratio (10) is:

$$\zeta_{r,y} = \mu \sqrt{\frac{2}{E}\, g_{yy}^2\, \pi_{r,y}}. \tag{13}$$

MSE $\pi_{r,y}$ is relatively easy to obtain using analytical or finite-element tools. With the help of Eq. (13) the damping ratio $\zeta_{r,y}$ can be predicted, given the

strain proportional damping parameter μ and the correct scaling coefficient g_{yy}. As will be shown in the following, the scaling coefficient is geometry dependent and can be, for a simple geometry, theoretically defined.

Relation between μ and β. The MSE π_r defined in (12), apart from a multiplication factor, also represents the r-th modal stiffness k_r [41]:

$$k_{r,y} = E\, I_{yy} \int_0^l \left(\frac{\partial^2 \phi_r(x)}{\partial x^2} \right)^2 \mathrm{d}x \qquad \pi_{r,y} = \frac{k_{r,y}}{2} \tag{14}$$

Since the mode shape ϕ_r is mass normalised, the modal stiffness $k_{r,y}$ results:

$$k_{r,y} = \omega_{r,y}^2 \tag{15}$$

where $\omega_{r,y}$ is the r-th natural frequency of bending around the y direction. Substituting Eqs. (15) and (14) into Eq. (13) the damping ratio $\zeta_{r,y}$ can be written as:

$$\zeta_{r,y} = \frac{\mu}{\sqrt{E}}\, g_{yy}\, \omega_{nr,y}. \tag{16}$$

Comparing Eq. (16) and the viscous damping definition (4), with $\alpha = 0$, we obtain:

$$\beta = 2\, \frac{\mu}{\sqrt{E}}\, g_{yy} \tag{17}$$

Eq. (17) defines the relation between the stiffness viscous damping coefficient β, the material dissipation property μ and the beam geometry, which will be shown to be related to g_{yy}.

4.1. Geometry normalisation

For linear systems, it is reasonable to expect that the scaling coefficient g_{yy} in Eq. (13) would not change the damping ratio. Further, the same strain proportional damping parameter μ should properly describe the damping ratio in the case of changes in the geometry (*i.e.*, cross-section or length). Due to this, the scaling coefficient g_{yy} (13) will be shown to account for the geometry normalisation.

Cross-section influence. The scaling coefficient will first be discussed for the case of a Euler-Bernoulli beam oscillating in bending around the y and z directions. The constant cross-sections geometry is defined with the second moments of area I_{yy} and I_{zz}, see Fig 1.

If the bending vibrations around the y and z direction are researched uncoupled, then the r-th mode shape ϕ_r defines the displacement mode shapes $w_r(x)$ and $v_r(x)$, respectively:

$$w_r(x) = g_{yy}\,\phi_r(x), \qquad v_r(x) = g_{zz}\,\phi_r(x). \tag{18}$$

The displacements $w_r(x)$ and $v_r(x)$ are represented by the same mass-normalised mode shape $\phi_r(x)$, just scaled differently. The displacements $w_r(x)$ and $v_r(x)$ can also be obtained with a proper static external force $f_r(x)$. In general, the forces for the y and z directions differ; however, due to the fact that for a constant cross-section, the external force is proportional to the second derivative of the strain ε_{xx} (8), see [41]:

$$f_r(x) \propto \frac{\partial^4 \varphi_r(x)}{\partial x^4}, \tag{19}$$

the static force $f_r(x)$ for the displacements $w_r(x)$ and $v(x)$ are proportional, *i.e.*, they differ by an unknown scaling factor. In Eq. (19) $\varphi_r(x)$ is the mode shape normalised to the unitary maximum displacement in contrast to $\phi(x)$ which is mass normalised and therefore depends on the beam geometry.

If the same external force $f_r(x)$ is separately applied to the two beam directions y and z, the external work applied on the beam is statically converted to the potential energy[1]; for the y direction bending:

$$\int_0^l f_r(x)\, w_r(x)\, \mathrm{d}x = \frac{1}{2}\, E\, I_{yy} \int_0^l \left(\frac{\partial^2 w_r(x)}{\partial x^2} \right)^2 \mathrm{d}x \tag{20}$$

and the z direction bending:

$$\int_0^l f_r(x)\, v_r(x)\, \mathrm{d}x = \frac{1}{2}\, E\, I_{zz} \int_0^l \left(\frac{\partial^2 v_r(x)}{\partial x^2} \right)^2 \mathrm{d}x. \tag{21}$$

[1]Potential energy equals to the strain energy π (not to be confused with the modal strain energy π_r (12).

Using the definitions of the displacements $w_r(x)$ and $v_r(x)$ (18):

$$\int_0^l f_r(x)\, g_{yy}\, \phi_r(x)\, \mathrm{d}x = \frac{1}{2}\, E\, I_{yy} \int_0^l \left(\frac{\partial^2 (g_{yy}\, \phi_r(x))}{\partial x^2} \right)^2 \mathrm{d}x \tag{22}$$

$$\int_0^l f_r(x)\, g_{zz}\, \phi_r(x)\, \mathrm{d}x = \frac{1}{2}\, E\, I_{zz} \int_0^l \left(\frac{\partial^2 (g_{zz}\, \phi_r(x))}{\partial x^2} \right)^2 \mathrm{d}x \tag{23}$$

where g_{yy} and g_{zz} are the two unknown scaling constants necessary to scale the mass-normalised mode shape $\phi_r(x)$ to the physical displacements $w(x)$ and $v(x)$, respectively.

If the constants g_{yy} and g_{zz} are extracted from the integrals in Eqs. (22) and (23), the following equations are obtained:

$$A = g_{yy}\, I_{yy}\, B \qquad A = g_{zz}\, I_{zz}\, B, \tag{24}$$

where:

$$A = \int_0^l f_r(x)\, \phi_r(x)\, \mathrm{d}x \qquad B = \frac{1}{2}\, E \int_0^l \left(\frac{\partial^2 \phi_r(x)}{\partial x^2} \right)^2 \mathrm{d}x. \tag{25}$$

From Eq. (24) it follows:

$$\frac{g_{zz}}{g_{yy}} = \frac{I_{yy}}{I_{zz}}. \tag{26}$$

Eq. (26) defines the ratio between the scaling coefficients; however, the absolute value is arbitrary. To have the scaling coefficients exactly defined, this research additionally imposes:

$$g_{zz}\, g_{yy} = 1. \tag{27}$$

Length influence. Two beams of length l_1 and l_2 with constant second moment of area I_{yy} are researched for bending around the y direction. The beams are loaded with the external forces $f_{1,r}(x)$ and $f_{2,r}(x)$. The loads $f_{1,r}(x)$ and $f_{2,r}(x)$ are proportional to the unitary maximum displacement normalised mode shape (19), thus with same amplitude and qualitatively with the same shape, squeesed to different lengths.

If the static external forces $f_{1,r}(x)$ and $f_{2,r}(x)$ are applied to the two beams in the z directions, the external work applied on the beam is converted to the

potential energy:

$$\int_0^{l_1} f_{1,r}(x)\, w_{1,r}(x)\, \mathrm{d}x = \frac{1}{2}\, E\, I_{yy} \int_0^{l_1} \left(\frac{\partial^2 w_{1,r}\,(x)}{\partial x^2} \right)^2 \mathrm{d}x \tag{28}$$

$$\int_0^{l_2} f_{2,r}(x)\, w_{2,r}(x)\, \mathrm{d}x = \frac{1}{2}\, E\, I_{yy} \int_0^{l_2} \left(\frac{\partial^2 w_{2,r}(x)}{\partial x^2} \right)^2 \mathrm{d}x \tag{29}$$

Using the definitions of the displacements $w_r(x)$ and $v_r(x)$ (18):

$$\int_0^{l_1} f_{1,r}(x)\, g_{yy,1}\, \phi_{1,r}(x)\, \mathrm{d}x = \frac{1}{2}\, E\, I_{yy} \int_0^{l_1} \left(\frac{\partial^2 (g_{yy,1}\, \phi_{1,r}(x))}{\partial x^2} \right)^2 \mathrm{d}x \tag{30}$$

$$\int_0^{l_2} f_{2,r}(x)\, g_{yy,2}\, \phi_{2,r}(x)\, \mathrm{d}x = \frac{1}{2}\, E\, I_{yy} \int_0^{l_2} \left(\frac{\partial^2 (g_{yy,2}\, \phi_{2,r}(x))}{\partial x^2} \right)^2 \mathrm{d}x \tag{31}$$

To generalise Eq.s (30) and (31) a normalised length coordinate χ is introduced:

$$\chi = \frac{x}{l}, \qquad \chi \in [0, 1]. \tag{32}$$

With the normalised variable χ, the mass normalised mode shape and the applied force are defined as (for details, see Eqs. (A.4) and (A.6) in Appendix A):

$$\psi_r(\chi) = \sqrt{l}\, \phi_r(x), \qquad f_r\,(\chi) \propto l^4\, f_r(x). \tag{33}$$

Introducing $\psi_r(\chi)$ and $f_r\,(\chi)$ to Eqs. (30) and (31):

$$\int_0^1 \frac{f_r(\chi)}{l_1^4}\, g_{yy,1}\, \frac{\psi_r(\chi)}{\sqrt{l_1}} l_1 \mathrm{d}\chi = \frac{1}{2}\, E\, I_{yy}\, g_{yy,1}^2 \int_0^1 \left(\frac{1}{l_1^2} \frac{\partial^2 \left(\frac{\psi_r(\chi)}{\sqrt{l_1}} \right)}{\partial \chi^2} \right)^2 l_1\, \mathrm{d}\chi \tag{34}$$

$$\int_0^1 \frac{f_r(\chi)}{l_2^4}\, g_{yy,1}\, \frac{\psi_r(\chi)}{\sqrt{l_2}}\, l_2\, \mathrm{d}\chi = \frac{1}{2}\, E\, I_{yy}\, g_{yy,2}^2 \int_0^1 \left(\frac{1}{l_2^2} \frac{\partial^2 \left(\frac{\psi_r(\chi)}{\sqrt{l_2}} \right)}{\partial \chi^2} \right)^2 l_2\, \mathrm{d}\chi \tag{35}$$

Eqs. (34) and (35) can be written in compact form as:

$$C = \frac{g_{yy,1}}{\sqrt{l_1}}\, D \qquad C = \frac{g_{yy,2}}{\sqrt{l_2}}\, D, \tag{36}$$

where:

$$C = \int_0^1 f_r(\chi)\, \psi_r(\chi)\, \mathrm{d}x \qquad D = \frac{1}{2}\, E\, I_{yy} \int_0^1 \left(\frac{\partial^2 \psi_r(\chi)}{\partial x^2} \right)^2 \mathrm{d}x. \tag{37}$$

From Eq. (36) it follows:

$$\frac{g_{yy,1}}{\sqrt{l_1}} = \frac{g_{yy,2}}{\sqrt{l_2}} \tag{38}$$

which defines the relation between the scaling factor g_{yy} and the beam length l.

Based on Eqs. (26) and (27), the generalised, length l dependent, scaling factors g_{yy} and g_{zz} are:

$$g_{yy}(l) = \sqrt{\frac{I_{zz}}{l\, I_{yy}}} \qquad g_{zz}(l) = \sqrt{\frac{I_{yy}}{l\, I_{zz}}} \tag{39}$$

4.2. Generalised strain proportional damping ratio

The relation between the strain related to the r-th mode shape and its damping ratio ζ_r in Eq. (13) can be generalised using the definition of the scaling coefficients g_{yy} and g_{zz} (39):

$$\zeta_{r,y} = \mu \sqrt{\frac{2}{E} \frac{I_{yy}}{l\, I_{zz}} \pi_{r,y}} \qquad \zeta_{r,z} = \mu \sqrt{\frac{2}{E} \frac{I_{zz}}{l\, I_{yy}} \pi_{r,z}} \tag{40}$$

where μ is the material property describing the dissipation ability, E is the modulus of elasticity, $\pi_{r,y}$ and $\pi_{r,z}$ are the MSE (normalised to unitary modal mass) of the r-th mode shape for bending around the y and z direction, respectively. I_{yy} and I_{zz} are the second moment of area.

Eq. (40) is based on the unitary modal mass-normalised mode shapes ϕ_r; however, if the MSE Π_r is computed using a mode shape Ψ_r normalised to a an arbitrary modal mass $\tilde{m}_r \neq 1$, then the damping ratio is [48]:

$$\zeta_{r,y} = \mu \sqrt{\frac{2}{E} \frac{I_{yy}}{l\, I_{zz}} \frac{\Pi_{r,y}}{\tilde{m}_{r,y}}} \qquad \zeta_{r,z} = \mu \sqrt{\frac{2}{E} \frac{I_{zz}}{l\, I_{yy}} \frac{\Pi_{r,z}}{\tilde{m}_{r,z}}} \tag{41}$$

where, as expected, the material property μ does not change with the mode-shape normalisation.

5. Experimental research

The strain proportional damping ratio, as proposed for a constant cross-section beam in Eq. (40), will here be used on real structures and compared to established damping models.

Nine beams are studied, with different cross-sections, lengths, materials and mode shapes. The geometrical and material properties of the studied beams are reported in Tab. 1.

Table 1: Geometry and material of the beam specimens

Specimen	$2\,b$ [mm]	$2h$ [mm]	t [mm]	l [mm]	**Material**
1	40	15	-	1000	aluminium
2	30	15	-	1000	aluminium
3	20	10	-	1000	aluminium
4	20	10	-	600	aluminium
5	20	10	-	398	aluminium
6	30	20	2	600	Laminated steel
7	40	20	2	600	Laminated steel-magnesium
8	30	20	-	500	Stainless steel
9	30	20	-	500	Stainless steel (with notch)

5.1. Experimental setup

The beams are tested in the free-free condition so that the damping due to constraints is minimised and dissipation is only due to the material's internal friction. The specimens are hung with long ropes in the direction orthogonal to the beam bending modes, as shown in Fig. 2. The hanging points are at 10% and 90% of the beam length l. The beams are excited with a PCB 086E80 miniature instrumented hammer at three locations: 20%, 50% and 70% of the beam length l. The response is measured with a Polytec PDV 100 vibrometer at 70% of the beam length l. Velocities and force are acquired using a NI CompactDaq and NI-9234 analog acquisition module for 1 second with a sampling frequency of 51200 Hz.

The damping ratios were identified using Least Square Complex Frequency (LSCF) domain [49] and logarithmic decrement [50] methods. The results of the two damping-identification methods do not show significant deviations, and all the following results are obtained using the LSCF method. A force window

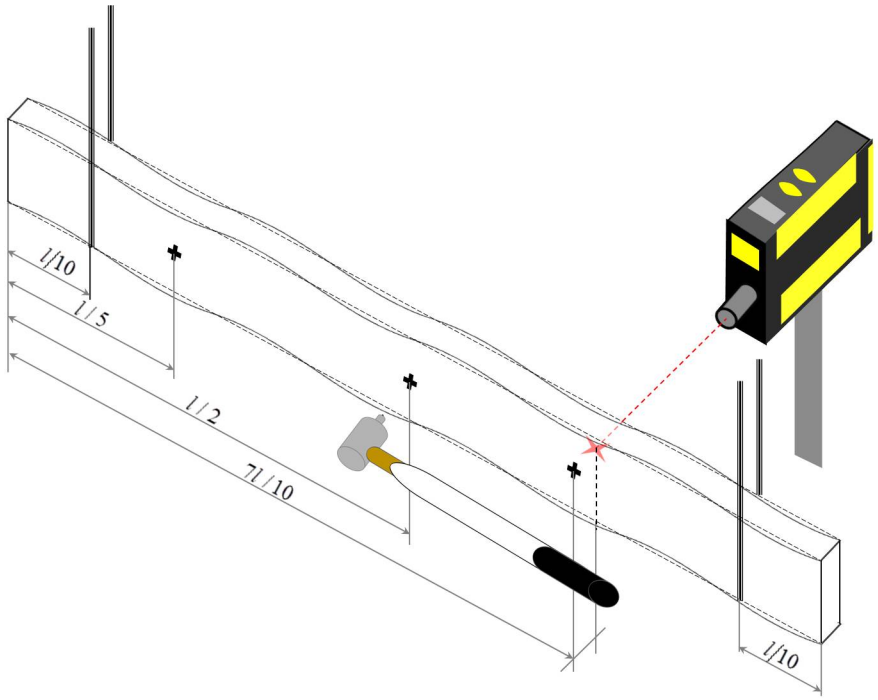

Figure 2: Experimental setup

is applied to the excitation data and the exponential window to the responses. Damping ratios are identified for the bending modes in the first 6 kHz. The identified damping ratios are compensated for the exponential window effect [51]. Table 2 lists the number of bending modes identified in the first 6 kHz; in total 127 different mode shapes were considered resulting in 127 experimentally identified damping ratios.

The experimentally identified damping ratios ζ_r^{exp} represent the effects of both the internal friction and the air damping [52]. The air damping can be analytically evaluated for the free-free beam [53] using Blevins' equation for fluid damping [54]:

$$\zeta_{air} = \frac{1}{2} \frac{\rho_{air}\, b^2}{m/l} \frac{V}{\omega_r\, b} C_D \tag{42}$$

where ρ_{air} is the air density, b is the width of the face in the plane of vibration, V is the velocity and C_D is the drag coefficient ($C_D = 2.08$ was used for the

Table 2: Experimentally identified bending modes

Specimen	y bending	z bending
1	12	8
2	12	9
3	15	11
4	9	6
5	6	4
6	6	4
7	5	3
8	6	4
9	7	-

tested beam's geometry). With Eq. (42) the air-damping is estimated to be orders of magnitude smaller than the identified damping in all the analysed cases, and therefore the air damping is neglected.

5.2. Change in geometry

Aluminium beams. Five aluminium beams from the same batch, but with different geometries, #1, #2, #3, #4 and #5, are experimentally tested, see Tab. 1 and Fig. 3. According to the theoretical model (5), the material damping parameter μ is expected to be a constant. The bending vibrations are experimentally investigated in both the y and z directions.

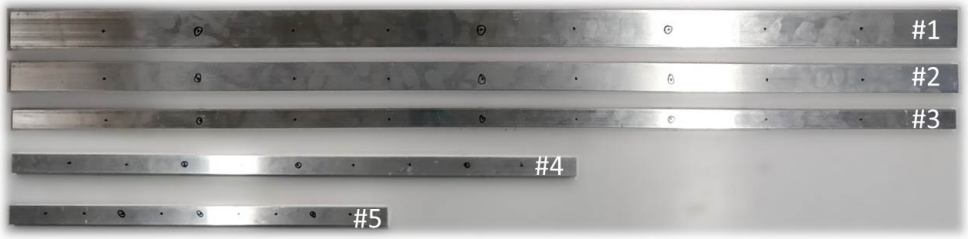

Figure 3: Aluminium beam specimens

Specimens #1, #2 and #3 have the same length $l = 1$ m; therefore, only

the cross-section effects the scaling factor g (26). Specimens #4 and #5 have a different length l and are used to validate the length's influence on the scaling factor g (39).

The stain proportional damping model (40) is used here to identify the material damping parameter μ from the experimentally measured damping ratio ζ_r^{exp} and the MSE π_r. MSE (12) is obtained here analytically from Euler-Bernoulli theory. Eq. (40) can be written for bending around the y and the z directions as:

$$\begin{bmatrix} \zeta_{y,1}^{exp} \\ \vdots \\ \zeta_{y,m}^{exp} \end{bmatrix} = \mu \begin{bmatrix} \sqrt{\frac{2}{E}\frac{I_{yy}}{lI_{zz}}\pi_{1,y}} \\ \vdots \\ \sqrt{\frac{2}{E}\frac{I_{yy}}{lI_{zz}}\pi_{m,y}} \end{bmatrix}, \qquad \begin{bmatrix} \zeta_{z,1}^{exp} \\ \vdots \\ \zeta_{z,m}^{exp} \end{bmatrix} = \mu \begin{bmatrix} \sqrt{\frac{2}{E}\frac{I_{zz}}{lI_{yy}}\pi_{1,z}} \\ \vdots \\ \sqrt{\frac{2}{E}\frac{I_{zz}}{lI_{yy}}\pi_{m,z}} \end{bmatrix} \tag{43}$$

where m is the number of considered mode shapes and $E = 65.6$ MPa for the considered material. The μ value is obtained from Eq. (43) in a least-squares sense for each direction of the beams' bending vibrations. The identified values of the μ material constant are shown in Fig. 4.

The second moment of area is, in the analysed bending directions of the beam, significantly different and so are the natural frequencies. However, as the strain proportional damping model predicts, the material property μ is almost the same for both directions. These results support the assumption of a constant material property μ as the proportionality coefficient between the damping ratio and the strain field in Eq. (40). The value μ for the aluminium results was $\mu_{Al} = (1.87 \pm 0.15) \cdot 10^{-3}\,\mathrm{m}^{-3/2}$.

The material property mean value μ required in Eq. (40) is now known for aluminium material $\mu_{Al} = 1.87 \cdot 10^{-3}\,\mathrm{m}^{-3/2}$ and can be used to numerically predict damping ratios ζ_r of beams bending modes, independently of the cross-section and the beam length. Moreover, once material property μ_{Al} is known, there is no necessity for experimental data anymore. In contrast: if damping would be modelled using the classical viscous damping approach (4), the viscous damping coefficients α and β obtained experimentally would be different for each

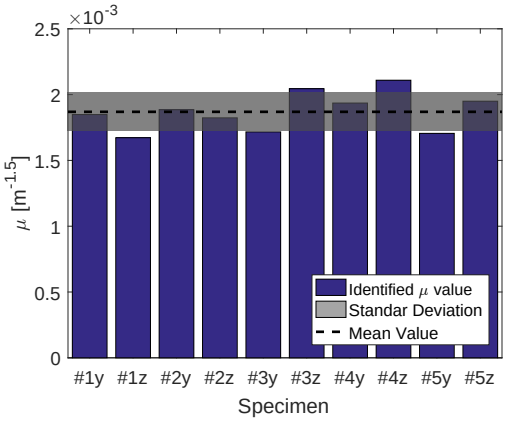

Figure 4: Identified μ value for aluminium beams

cross-section, each length and each material.

Assuming $\alpha = 0$ [11], the stiffness viscous proportionality coefficient β required to fit the experimental damping ratios is different for each aluminium beam; their values, given in Tab. 3, are fitted to the experimental data for each beam. μ in Tab. 3 is derived using Eq. (17), the obtained values are close to the identified μ_{Al}, however they are more spread. This difference is expected since the experimental derivation of the MSE π_r, used in Eq.(43), is much more robust than the experimental fitting of β.

Table 3: Stiffness viscous damping coefficents β and derived μ

Specimen	β $[10^{-8}\text{rad/s}]$	μ $[10^{-3}\text{m}^{-1.5}]$	**Specimen**	β $[10^{-8}\text{rad/s}]$	μ $[10^{-3}\text{m}^{-1.5}]$
1y	3.39	1.7	1z	0.68	2.2
2y	2.68	1.7	2z	0.83	2.4
3y	1.94	1.2	3z	0.65	1.6
4y	2.30	1.1	4z	0.88	1.7
5y	2.05	0.8	5z	0.66	1.0

For the samples #3 and #4 vibrating in bending around the y direction the detailed analysis is shown in Figs. 5 and 6. The damping ratios are numerically

obtained with both the strain proportional damping (40) and the standard viscous damping model (4), with $\alpha = 0$ [11]. The estimated damping ratios using strain proportional and viscous proportional damping are very close to each other and reproduce quite well the experimental damping ratio ζ_r^{exp} trend, except for the first mode damping ζ_1^{exp} which is higher. This is probably due to the dissipation effect of the long ropes used to hang the beams. The results for the other specimens are qualitatively the same.

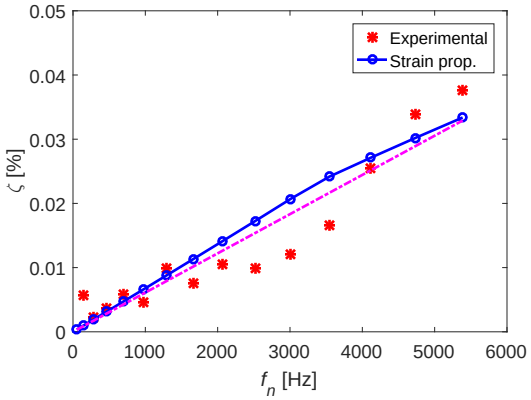

Figure 5: Damping ratio ζ_r trend for beam #3 bending around the y direction

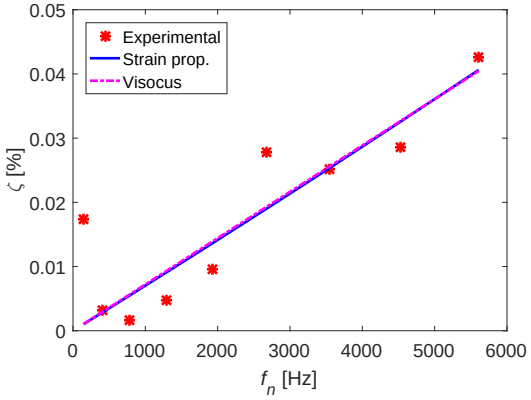

Figure 6: Damping ratio ζ_r trend for beam #4 bending around the y direction

Box cross-section. In this section the strain-proportionality approach is applied to steel beams with a box cross-section, in order to test the method on more complex cross-sections, see Fig. (7) and in Tab. 1.

Figure 7: Laminated steel box beam

The two beams are manufactured with different steel alloys; therefore, different values for the material property μ are expected. Specimen #6 is produced with steel, while specimen #7 is produced with a steel-magnesium alloy, both are manufactured as folded and welded laminated sheets. The two beams are tested in both vibration planes. The parameter μ is identified using Eq. (43), and the obtained values are shown in Fig. 8. The strain-proportional damping parameter μ is almost the same in the two vibration planes of the same beam and slightly different between the two beams, as expected.

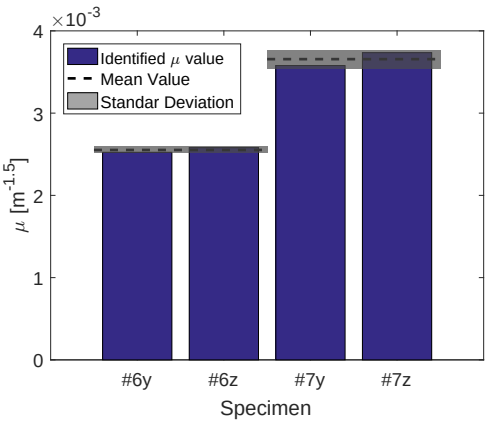

Figure 8: Identified μ value for laminated steel beams

5.3. Beam with a notch

In this section the effect of a significantly changed MSE due to a notch in the beam is analysed. Here, the MSE is obtained using a numerical simulation. Two extruded stainless-steel beams of the same batch material, specimens #8 and #9, with the same cross-section and the same length are analysed, see Fig. 9 and Tab. 1. The notch in the middle of the beam #9 significantly changes the natural frequencies $\omega_{n,r}$, mode shapes ϕ_r and damping ratios ζ_r. Fig. (10) shows a selected frequency-response function (same excitation/response pair). Since the two beams are of the same material, the same μ values are expected, although the modal properties are different.

Figure 9: Twin steel beams

The estimation of the μ values is performed using Eq. (40), in the least-squares form (43). The mode shapes of the cracked beam are numerically evaluated using a FE model of the cracked beam, with Euler-Bernoulli beam elements. The hypothesis of an infinity small crack is assumed for the computation of the MSE π_r of the cracked beam. Specimen #8 is tested in both directions; while the notched beam, specimen #9, is tested only for the y direction bending, since the presence of the notch couples the bending and torsional modes in the other plane. The identified μ values are shown in Fig. 11.

As expected, the identified μ values are almost the same for the three sets of data. The damping ratio ζ_r of the two beams vibrating around the y bending

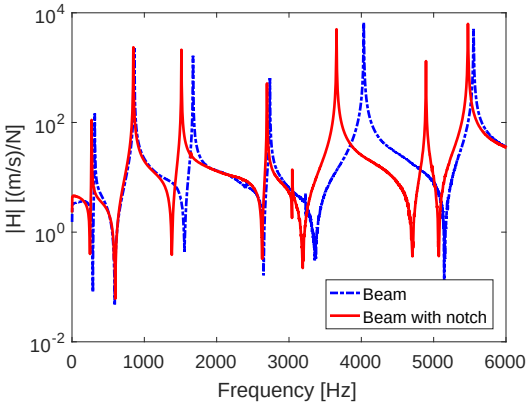

Figure 10: Twin beams FRF comparison

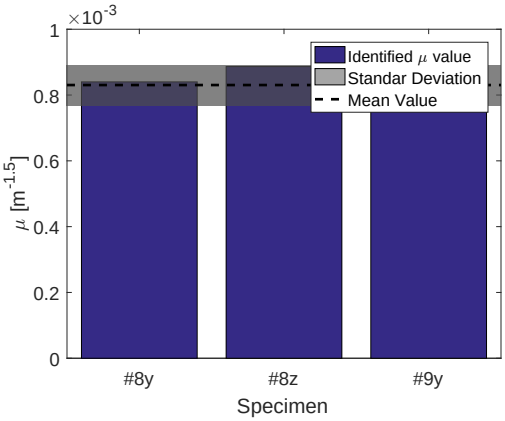

Figure 11: Material property k for the steel twin beams

are compared in Fig. 12. The mean μ value is used to predict the damping ratios of both the two beams. The results obtained are very similar to the classic β proportional viscous damping, which however requires the fitting of β on each system and therefore use two different β values. The damping ratios of the notched beam are generally lower than the twin beam, this suggests a lower level of the global strain field in the notched beam.

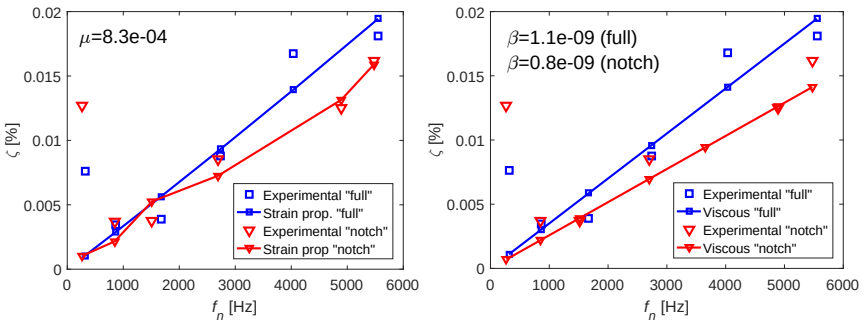

Figure 12: Experimental and predicted damping ratio for the twin steel beams: strain-proportional damping (left), viscous damping (right).

6. Conclusion

A new approach to modal-damping-ratio estimation is proposed in this research. The basic assumption is that the r-th modal damping ratio ζ_r can be related to the modal strain energy (MSE) π_r via the newly introduced strain proportional damping parameter μ. Based on this idea, no damping energy can be generated at locations where there is no material strain (this is not the case in most damping models, i.e., damping energy density is present in the maximum or node of strain modes).

The proposed theoretical model is researched in detail with the Euler-Bernoulli beam theory and confirms to give consistent results on several experimental test cases. Five different aluminium beam specimens with different cross-sections, inertia values and lengths were shown to have the same material damping parameter μ. Further experiments were prepared on box cross-section beams made of different materials; despite the differences in cross-section, the material damping parameter was shown to correctly estimate the damping ratio in perpendicular directions of the bending vibrations. The last experiment was based on a notched vs. notch-free sample; this sample required a numerical estimation of the MSE and additionally confirmed that damping ratios can be correctly estimated based on the material damping parameter μ

The modal damping ratio is, based on the viscous proportional damping

theory, frequently estimated via the mass α and the stiffness β proportionality parameters. Parameters α and β are structure-specific and cannot be generalised to arbitrary shapes.

In this research the proposed material-damping parameter μ was theoretically generalised for the Euler-Bernoulli beam. It was confirmed that, based on the material damping parameter μ, the damping ratios of arbitrary modes and Euler-Bernoulli beam of arbitrary geometry can be theoretically predicted correctly.

Acknowledgement

The authors acknowledge the partial financial support from the Slovenian Research Agency (research core funding no. P2-0263 and project J2-1730).

References

[1] R. E. D. Bishop, The Treatment of Damping Forces in Vibration Theory, The Journal of the Royal Aeronautical Society 59 (539) (1955) 738–742 (1955). doi:10.1017/S0368393100117122.

[2] S. Adhikari, Damping Models for Structural Vibration, Ph.D. thesis, Cambridge University (2000).

[3] P. Balasubramanian, G. Ferrari, M. Amabili, Identification of the viscoelastic response and nonlinear damping of a rubber plate in nonlinear vibration regime, Mechanical Systems and Signal Processing 111 (2018) 376–398 (oct 2018). doi:10.1016/J.YMSSP.2018.03.061.
URL https://www.sciencedirect.com/science/article/pii/S0888327018301882{#}b0005

[4] F. Mastroddi, F. Martarelli, M. Eugeni, C. Riso, Time- and frequency-domain linear viscoelastic modeling of highly damped aerospace structures, Mechanical Systems and Signal Processing 122 (2019) 42–55 (may 2019).

doi:10.1016/J.YMSSP.2018.12.023.
URL https://www.sciencedirect.com/science/article/pii/S0888327018307982

[5] J. Rayleigh, The Theory of Sound - Vol.1, no. v. 1 in The Theory of Sound, Macmillan, 1877 (1877).

[6] J. W. Strutt, Some General Theorems relating to Vibrations, Proceedings of the London Mathematical Society s1-4 (1) (1871) 357–368 (nov 1871). doi:10.1112/plms/s1-4.1.357.
URL http://doi.wiley.com/10.1112/plms/s1-4.1.357

[7] T. K. Caughey, M. E. J. O'Kelly, Classical normal modes in damped linear dynamic systems, Journal of Applied Mechanics 32 (3) (1965) 583–588 (sep 1965).

[8] S. Adhikari, Damping modelling using generalized proportional damping, Journal of Sound and Vibration 293 (1-2) (2006) 156–170 (may 2006). doi:10.1016/J.JSV.2005.09.034.
URL https://www.sciencedirect.com/science/article/pii/S0022460X05006942

[9] M. Géradin, D. J. Rixen, Mechanical Vibrations: Theory and Application to Structural Dynamics, 3rd Edition, John Wiley & Sons, 2015 (2015).

[10] V. Anes, Y. Lage, M. Vieira, N. Maia, M. Freitas, L. Reis, Torsional and axial damping properties of the az31b-f magnesium alloy, Mechanical Systems and Signal Processing 79 (2016) 112 – 122, special Issue from ICEDyn 2015 (2016). doi:https://doi.org/10.1016/j.ymssp.2016.02.040.
URL http://www.sciencedirect.com/science/article/pii/S0888327016000911

[11] A. M. Kabe, B. H. Sako, Issues with proportional damping, AIAA Journal 54 (9) (2016) 2864–2868 (2016). doi:10.2514/1.J054080.

[12] S. G. Kelly, Fundamentals of Mechanical Vibrations, McGraw-Hill series in mechanical engineering, McGraw-Hill, 2000 (2000).

[13] E. Erduran, Evaluation of Rayleigh damping and its influence on engineering demand parameter estimates, Earthquake Engineering and Structural Dynamics 41 (14) (2012) 1905–1919 (2012). doi:10.1002/eqe.2164.

[14] L. Zoghaib, P. O. Mattei, Damping analysis of a free aluminum plate, JVC/Journal of Vibration and Control 21 (11) (2013). doi:10.1177/1077546313507098.

[15] S. Nikolaev, S. Voronov, I. Kiselev, Estimation of damping model correctness using experimental modal analysis — JVE Journals.
URL https://www.jvejournals.com/article/15381

[16] C. Cruz, E. Miranda, Evaluation of the Rayleigh damping model for buildings, Engineering Structures 138 (2017) 324–336 (may 2017). doi:10.1016/J.ENGSTRUCT.2017.02.001.
URL https://www.sciencedirect.com/science/article/pii/S0141029616306885

[17] T. Theodorsen, I. E. Garrick, Mechanism of flutter a theoretical and experimental investigation of the flutter problem (1940).

[18] R. E. D. Bishop, D. C. Johnson, The Mechanics of Vibration, Cambridge University Press, 1960 (1960).

[19] F. Cortés, M. Elejabarrieta, An approximate numerical method for the complex eigenproblem in systems characterised by a structural damping matrix, Journal of Sound and Vibration 296 (1-2) (2006) 166–182 (sep 2006). doi:10.1016/J.JSV.2006.02.016.

[20] A. M. Baz, Active and Passive Vibration Damping, Wiley, 2019 (2019).

[21] D. J. McTavish, P. C. Hughes, Modeling of Linear Viscoelastic Space Structures, Journal of Vibration and Acoustics 115 (1) (1993) 103–110 (jan 1993). doi:10.1115/1.2930302.

[22] G. A. Lesieutre, E. Bianchini, Time Domain Modeling of Linear Viscoelasticity Using Anelastic Displacement Fields, Journal of Vibration and Acoustics 117 (4) (1995) 424–430 (oct 1995). doi:10.1115/1.2874474.

[23] R. L. Bagley, P. J. Torvik, Fractional calculus in the transient analysis of viscoelastically damped structures, AIAA Journal 23 (6) (1985) 918–925 (jun 1985). doi:10.2514/3.9007.

[24] C. Zener, Elasticity and anelasticity of metals, University of Chicago press, 1948 (1948).

[25] C. Bert, Material damping: An introductory review of mathematic measures and experimental technique, Journal of Sound and Vibration 29 (2) (1973) 129–153 (jul 1973). doi:10.1016/S0022-460X(73)80131-2.

[26] H. T. Banks, D. J. Inman, On Damping Mechanisms in Beams, Journal of Applied Mechanics 58 (3) (1991) 716–723 (sep 1991). doi:10.1115/1.2897253.

[27] A. E. H. Love, A Treatise on the Mathematical Theory of Elasticity, Cambridge University Press, 2013 (2013).
URL https://books.google.it/books?id=JFTbrz0Fs5UC

[28] D. L. Russell, 4. On Mathematical Models for the Elastic Beam with Frequency-Proportional Damping, in: Control and Estimation in Distributed Parameter Systems, Society for Industrial and Applied Mathematics, 1992, pp. 125–169 (jan 1992). doi:10.1137/1.9781611970982.ch4.
URL http://epubs.siam.org/doi/10.1137/1.9781611970982.ch4

[29] A. L. Kimball, D. E. Lovell, Internal Friction in Solids, Physical Review 30 (6) (1927) 948–959 (dec 1927). doi:10.1103/PhysRev.30.948.

[30] B. J. Lazan, A study with new equipment of the effects of fatigue stress on the damping capacity and elasticity of mild steel, Trans. Am. Soc. Metals 4 (1950) 499–558 (1950).

[31] F. Sánchez Iglesias, A. Fernández López, Rayleigh damping parameters estimation using hammer impact tests, Mechanical Systems and Signal Processing 135 (2020) 106391 (jan 2020). doi:10.1016/J.YMSSP.2019.106391.
URL https://www.sciencedirect.com/science/article/pii/S0888327019306120

[32] I. Yılmaz, E. Arslan, E. Ç. Kiziltas, K. Çavdar, Development of a prediction method of Rayleigh damping coefficients for free layer damping coatings through machine learning algorithms, International Journal of Mechanical Sciences (2019) 105237 (oct 2019). doi:10.1016/J.IJMECSCI.2019.105237.
URL https://www.sciencedirect.com/science/article/pii/S0020740319313487

[33] F. Sarbinowski, R. Labudzki, R. Talar, A. Patalas, Application of a vision system to determine the Rayleigh damping coefficients of materials used in stereolithography, in: IOP Conference Series: Materials Science and Engineering, Vol. 393, Institute of Physics Publishing, 2018 (aug 2018). doi:10.1088/1757-899X/393/1/012087.

[34] M. Hamdaoui, K. Ledi, G. Robin, E. Daya, Identification of frequency-dependent viscoelastic damped structures using an adjoint method, Journal of Sound and Vibration 453 (2019) 237–252 (aug 2019). doi:10.1016/J.JSV.2019.04.022.
URL https://www.sciencedirect.com/science/article/pii/S0022460X19302330

[35] L. Su, S.-Q. Mei, Y.-H. Pan, Y.-F. Wang, Experimental identification of exponential damping for reinforced concrete cantilever beams, Engineering Structures 186 (2019) 161–169 (may 2019). doi:10.1016/J.ENGSTRUCT.2019.02.015.

URL https://www.sciencedirect.com/science/article/pii/S0141029618322880

[36] H. M. Nghiem, N.-Y. Chang, A new viscous damping formulation for 1D linear site response analysis, Soil Dynamics and Earthquake Engineering 127 (2019) 105860 (dec 2019). doi:10.1016/J.SOILDYN.2019.105860.
URL https://www.sciencedirect.com/science/article/pii/S0267726118304147

[37] T. Heitz, C. Giry, B. Richard, F. Ragueneau, Identification of an equivalent viscous damping function depending on engineering demand parameters, Engineering Structures 188 (2019) 637–649 (jun 2019). doi:10.1016/J.ENGSTRUCT.2019.03.058.
URL https://www.sciencedirect.com/science/article/pii/S0141029618305121

[38] P. Ficzere, L. Borbás, Experimental dynamical analysis of specimens' material properties manufactured by additive technologies, Materials Today: Proceedings 12 (2019) 352–357 (jan 2019). doi:10.1016/J.MATPR.2019.03.135.
URL https://www.sciencedirect.com/science/article/pii/S2214785319304948

[39] M. Mihalec, J. Javh, F. Cianetti, M. Moretti, G. Rossi, J. Slavič, M. Boltežar, Damping heat coefficient – Theoretical and experimental research on a vibrating beam, Journal of Sound and Vibration (2017) 13–21 (jul 2017). doi:10.1016/J.JSV.2017.04.023.

[40] T. Kranjc, J. Slavič, M. Boltežar, A comparison of strain and classic experimental modal analysis, Journal of Vibration and Control 22 (2) (2016) 371–381 (2016). arXiv:https://doi.org/10.1177/1077546314533137, doi:10.1177/1077546314533137.
URL https://doi.org/10.1177/1077546314533137

[41] S. S. Rao, Vibration of Continuous Systems, Wiley, 2007 (2007).

[42] L. Meirovitch, Analytical methods in vibrations, Macmillan series in advanced mathematics and theoretical physics, Macmillan, 1967 (1967).
URL https://books.google.it/books?id=H2ortwEACAAJ

[43] L. Maxit, Analysis of the modal energy distribution of an excited vibrating panel coupled with a heavy fluid cavity by a dual modal formulation, Journal of Sound and Vibration 332 (25) (2013) 6703–6724 (dec 2013). doi:10.1016/J.JSV.2013.07.020.
URL https://www.sciencedirect.com/science/article/pii/S0022460X13006342

[44] S. K. Tolani, R. D. Rocke, Modal truncation of substructures used in free vibration analysis, Journal of Manufacturing Science and Engineering, Transactions of the ASME 98 (3) (1976) 827–834 (1976). doi:10.1115/1.3439037.

[45] E. E. Ungar, E. M. Kerwin, Loss Factors of Viscoelastic Systems in Terms of Energy Concepts, The Journal of the Acoustical Society of America 34 (7) (1962) 954–957 (jul 1962). doi:10.1121/1.1918227.
URL http://asa.scitation.org/doi/10.1121/1.1918227

[46] G. Mulder, On strain-rate independent damping in continuum mechanics, Journal of Sound and Vibration 407 (2017) 240–252 (oct 2017). doi:10.1016/J.JSV.2017.06.028.

[47] F. L. M. Dos Santos, B. Peeters, W. Desmet, L. C. S. Góes, Strain-based experimental modal analysis: New concepts and practical aspects, in: Proceedings of ISMA 2016 - International Conference on Noise and Vibration Engineering and USD2016 - International Conference on Uncertainty in Structural Dynamics, 2016, pp. 2263–2277 (2016).

[48] N. Kumar, S. Singh, Vibration control of curved panel using smart damping, Mechanical Systems and Signal Processing 30 (2012) 232–247

(jul 2012). doi:10.1016/J.YMSSP.2011.12.012.
URL https://www.sciencedirect.com/science/article/pii/S0888327011005280

[49] P. Verboven, Frequency-domain system identification for modal analysis, Vrije Universiteit Brussel, Brussels (2002).

[50] D. J. Inman, Engineering Vibration, Pearson, 2014 (2014).

[51] W. Fladung, R. Rost, Application and correction of the exponential window for frequency response functions, Mechanical Systems and Signal Processing 11 (1) (1997) 23–36 (jan 1997). doi:10.1006/MSSP.1996.0084.
URL https://www.sciencedirect.com/science/article/pii/S0888327096900849

[52] M. Wesolowski, E. Barkanov, Improving material damping characterization of a laminated plate, Journal of Sound and Vibration 462 (2019) 114928 (dec 2019). doi:10.1016/J.JSV.2019.114928.
URL https://www.sciencedirect.com/science/article/pii/S0022460X19304900

[53] G. T. Spirnak, J. R. Vinson, The Effect of Temperature on the Material Damping of Graphite/Epoxy Composites in a Simulated Space Environment, Journal of Engineering Materials and Technology 112 (3) (1990) 277–279 (jul 1990). doi:10.1115/1.2903323.

[54] R. D. Blevins, Flow-induced Vibration, Krieger Publishing Company, 2001 (2001).

Appendix A. Length normalisation of mode shape and force load

The mass normalised mode shape ϕ_r can be defined as the ratio between the unitary displacement mode shape φ_r and the related modal mass m_r [42]:

$$\phi_r(x) = \frac{\varphi_r(x)}{\sqrt{m_r(x)}} = \frac{A_r \cos\left(\frac{\lambda_r}{l}x\right) + B_r \sin\left(\frac{\lambda_r}{l}x\right) + C_r \cosh\left(\frac{\lambda_r}{l}x\right) + D_r \sinh\left(\frac{\lambda_r}{l}x\right)}{\sqrt{\rho A \int_0^l \varphi_r(x)^2 \mathrm{d}x}} \tag{A.1}$$

where A_r,B_r,C_r and D_r depend on the beam boundary conditions, and λ_r is the r-th of the characteristic equation dependent on the boundary conditions. The variable substitution (32) for the unitary displacement mode shape φ_r leads to the definition of the unitary maximum displacement mode-shapes in χ domain:

$$\tilde{\varphi}_r(\chi) = A_r \cos(\lambda_r \chi) + B_r \sin(\lambda_r \chi) + C_r \cosh(\lambda_r \chi) + D_r \sinh(\lambda_r \chi) \quad \text{(A.2)}$$

The modal mass in χ domain can be defined as:

$$m_r(\chi) = \rho A \int_0^1 \tilde{\varphi}_r(\chi)^2 \, l \, \mathrm{d}\chi \quad \text{(A.3)}$$

If the (A.2) and (A.3) are replaced in the definition of unitary modal mass mode shape (A.1), it can be defined in χ domain as:

$$\phi_r(x) = \frac{\tilde{\varphi}_r(\chi)}{\sqrt{m_r(\chi)}} = \frac{\psi_r(\chi)}{\sqrt{l}} \quad \text{(A.4)}$$

where the mode shape $\psi_r(\chi)$ does not depend on beam length and is defined as:

$$\psi_r(\chi) = \frac{\tilde{\varphi}(\chi)}{\sqrt{\rho A \int_0^1 \tilde{\varphi}(\chi)^2 \, \mathrm{d}\chi}} \quad \text{(A.5)}$$

Remembering the definition of the applied force (19) and performing the variable substituting (32) it result:

$$f_r(x) \propto \frac{1}{l^4} \frac{\partial^4 \tilde{\varphi}_r(\chi)}{\partial \chi^4} = \frac{f_r(\chi)}{l^4} \quad \text{(A.6)}$$